Planetary and Space Science 109-110 (2015) 32–37

Contents lists available at ScienceDirect

Planetary and Space Science

journal homepage: www.elsevier.com/locate/pss

The shape of the Venusian bow shock at solar minimum and maximum: Revisit based on VEX observations

Lican Shan [a], Quanming Lu [a,*], Christian Mazelle [b], Can Huang [a], Tielong Zhang [a,c], Mingyu Wu [a], Xinliang Gao [a], Shui Wang [a]

[a] CAS Key Lab of Geoscience Environment, Department of Geophysics and Planetary Science, University of Science and Technology of China, Hefei 230026, China
[b] IRAP UPS-CNRS, Toulouse, France
[c] Space Research Institute, Austrian Academy of Sciences, Graz, Austria

ARTICLE INFO

Article history:
Received 30 October 2013
Received in revised form
15 January 2015
Accepted 19 January 2015
Available online 31 January 2015

Keywords:
Venus bow shock
Venus Express
Solar activity

ABSTRACT

Several factors control the bow shock position at Venus, including short-term period responses (solar wind dynamic pressure) and long-term period variations (solar activity). Based on Venus Express (VEX) observations, we revisit the influence of solar activity on the Venusian bow shock location, by accurately determining not only the shock terminator distance but also the subsolar point with a three-parameter fit (TPF) method. At the same time, VEX covers a larger range of solar zenith angles (SZA) at the Venusian bow shock (from about 10 to 135 degrees) than the Pioneer Venus Orbiter (PVO) spacecraft. Fitting results display that the Venusian bow shock is farther away from Venus at solar maximum than at solar minimum. The subsolar stand-off distance increases from 1.364 planetary radii at solar minimum to $1.459R_V$ at solar maximum, while the terminator shock distance changes from $2.087R_V$ to $2.146R_V$. Inspection of the bow shock and the induced magnetosphere boundary (IMB) locations clearly shows a positive correlation for every orbit, while the average bow shock location is not responsive to changes in the solar wind dynamic pressure.

1. Introduction

A shock plays an important role in converting upstream bulk flow energy into downstream thermal energy, across which the plasma speed decreases from super-magnetosonic upstream to sub-magnetosonic downstream. A planetary bow shock is formed when the high-speed solar wind interacts with the magnetosphere/ionosphere of a planet. Due to the lack of an intrinsic planetary magnetic field, the deflection of the solar wind at the Venusian bow shock is caused by an induced magnetosphere created by the interaction between the solar wind and the planetary ionosphere (Luhmann, 1986; and references therein). Although the radius of Venus is similar to that of Earth, the size of the Venusian bow shock is less than 1/10th of the size of the Earth's bow shock (Slavin et al., 1979a). In consideration of the dimension of the Venusian radius ($1R_V = 6051$ km), the shock is hanged tightly around the planet.

Since the Venusian bow shock was initially identified by the Mariner 5 satellite (Bridge et al., 1967), it has been studied by several spacecraft missions (Dolginov et al., 1968; Verigin et al., 1978; Zhang et al., 2006). Among them, the Pioneer Venus Orbiter (PVO) mission provided the longest duration for observations (~14 years). Based on the PVO observations, Slavin et al. (1979a) found that the bow shock terminator distance near solar maximum in 1978 and 1979 is about 2.44 R_V, while the Venera 9/10 observations showed that the bow shock terminator distance is 2.09 R_V near solar minimum in 1975 and 1976. After the shock terminator distance reached a maximum of 2.45 R_V at solar maximum in 1980, it began to decline steadily to 2.13 R_V at solar minimum in 1986 (Alexander and Russell, 1985; Russell et al., 1988; Zhang et al., 1990). Such a variation of the shock position was attributed to some effects of the solar cycle. As solar maximum approaches, simulations suggest that more neutral particles from the Venusian atmosphere have access to the magnetosheath (Gröller et al., 2010) and the extended planetary hot atomic oxygen corona covers the magnetosheath. Then more neutral particles are ionized due to the increase of solar EUV. Therefore, the additional mass added to the planetary magnetosheath plasma causes the bow shock to move outward. The existence of these additional particles (pickup ions) in the Venusian magnetosheath also leads to a weaker Venusian bow shock than its terrestrial analogue due to mass-loading (Russell et al., 1979; Lu et al., 2013), in a similar manner as for the Martian bow shock (Mazelle, 2004; and references therein), and a weaker

* Corresponding author.
E-mail address: qmlu@ustc.edu.cn (Q. Lu).

http://dx.doi.org/10.1016/j.pss.2015.01.004
0032-0633/

Venusian bow shock near solar maximum than near solar minimum.

However, due to orbital bias of PVO, its range of solar zenith angle (SZA) at the Venusian bow shock varies from ~60° to ~110°(Slavin et al., 1979b). The subsolar location of the Venusian bow shock fit is not covered by PVO observations and the best-fit technique for the bow shock location is only valid at the terminator plane. Venus Express (VEX) was launched on November 9, 2005 and reached Venus on April 11, 2006. It orbits Venus with a highly elliptical polar orbit that crosses the bow shock twice a day, and provides a sufficiently long duration for observations, which gives us another opportunity to investigate the effects of solar activity on the Venusian bow shock. In addition, compared with PVO, VEX covers a larger range of SZA (from ~10° to ~135°) at the Venusian bow shock, and is suitable to determine the bow shock locations at both the stand-off and terminator distances (Zhang et al., 2006; Martinecz et al., 2008; Whittaker et al., 2010). Therefore, the shape of the Venusian bow shock can be determined with the desired accuracy to undertake stand- off variation studies. In this paper, with magnetic field measurements from VEX, we revisit the influence of solar activity on the Venusian bow shock by comparing the shape of the shock at solar maximum and minimum. Moreover, in order to seek for correlations between shock locations and the induced magnetosphere boundary (IMB) location, we have fitted a sample of IMB locations with the same methods. A proxy previously used at Mars (Crider et al., 2003) is also used here for studying the influence of the variations of the solar wind dynamic pressure.

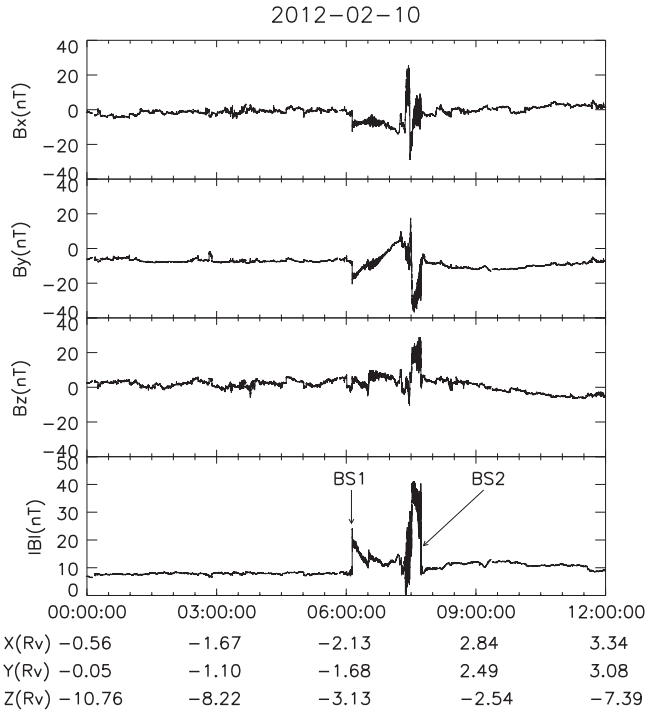

Fig. 1. 1 Hz sampling magnetic field measurements from VEX for 12 h on 10 February 2012. BS1 and BS2 represent the inbound and outbound shock crossing, respectively.

2. Observations

VEX has an elliptical polar orbit with a periapsis of 250–300 km altitude at 78°N, and the magnetometer MAG on board of VEX consists of two fluxgate sensors for a separation of magnetic effects of the spacecraft origin from the ambient space magnetic field (Zhang et al., 2006). Fig. 1 displays 1 Hz sampling magnetic field measurements from MAG on 10 February 2012, and the observations are presented in the Venus Solar Orbital (VSO) coordinates. X is aligned with the Venus to Sun direction, Y is oriented along the planet's orbital velocity and Z completes the direct coordinates system. Bow shocks are identified by a jump in the magnetic field amplitude with respect to the upstream region, and the locations are also compared with previous and subsequent orbits. For quasi-perpendicular bow shock, the medium of the ramp is selected as the shock location, while for the quasi-parallel one, we use the middle time of the transition interval between the upstream solar wind and magnetosheath. In the latter case, there is an error bar on the shock location, but we have checked that it has little influence on the present statistical study. The spacecraft encounters the inbound (BS1) and outbound shock crossings (BS2) at ~06:08:00 UT and ~07:43:28 UT, corresponding to the positions $(-2.10, -1.67, -2.78)R_V$ and $(1.14, 0.94, 0.64)R_V$, respectively. SZA at BS1 is 123°, and it is 45° for BS2. The shock angle θ_{Bn} (the angle between the interplanetary magnetic field and the shock normal) is calculated with the minimum variance analysis method (Sonnerup and Scherble, 1998). The values are 58° for BS1 and 69° for BS2. The ratios of the maximum to intermediate and intermediate to minimum eigenvalues are 2.1 and 4.9 for BS1, and 1.8 and 3.8 for BS2, respectively. The values of θ_{Bn} computed by magnetic coplanarity and Venusian bow shock model (Shan et al., 2013; and references therein) are 56° and 65° for BS1, and 61° and 65° for BS2, respectively.

After we have identified the shock positions in the VSO coordinates, we take account of Venus orbital motion (~35 km/s), and we transform the data into an aberrated solar ecliptic system, which has an assumed angle 4.7° aberration from VSO. The shape of the shock is then fitted with a conic section curve, and the equation for the conic section is

$$R = \frac{L}{1+\varepsilon \cos\theta} \quad (1)$$

where R is the observed bow shock distance from the conic focus, L is the conic section semi-latus rectum, ε is the eccentricity. There are two least-square fit methods: direct fit (DF) (Spreiter et al., 1970; Russell, 1977) and three-parameter fit (TPF) with a best fitted focus (Slavin et al., 1980; Slavin and Holzer, 1981). The former method is also called two-parameter fit. In the DF method, the focus of the conic section curve is assumed to be in the center of Venus. L and ε should be fitted. For the TPF method, the focus $(x_o, 0, 0)$ of the conic section curve is not assumed to be in the center of the Venus, and the three parameters L, ε and x_o should be fitted.

We have obtained 454 clear bow shock crossings at solar minimum (from August 2008 to May 2009) and 335 clear crossings at solar maximum (from May 2011 to February 2012). The averages of monthly sunspot numbers are 1.7 and 60.0 (from the website http://sidc.oma.be/sunspot-data/) during these two intervals. Fig. 2 shows the fits based on magnetic field measurements at solar minimum (Fig. 2a) and maximum (Fig. 2b) with DF (blue curves) and TPF methods (black and red curves). It is found that the mean of the absolute deviation (MAD) of TPF method is smaller than that of DF method. The calculated MAD with DF method is $0.182R_V$ at solar minimum and $0.208R_V$ at solar maximum, while it is $0.153R_V$ at solar minimum and $0.180R_V$ at solar maximum with TPF method. Because of the smaller errors, the TPF method is better to determine the influence of solar activity on the shape of the Venusian bow shock. Fig. 2c compares the shape of the Venusian bow shock at solar minimum and maximum fitted with TPF method.

The IMB locations on the dayside used in the present study are also displayed (green) in Fig. 2a and b as well as the results of the DF method (green curves). IMB crossings has been determined

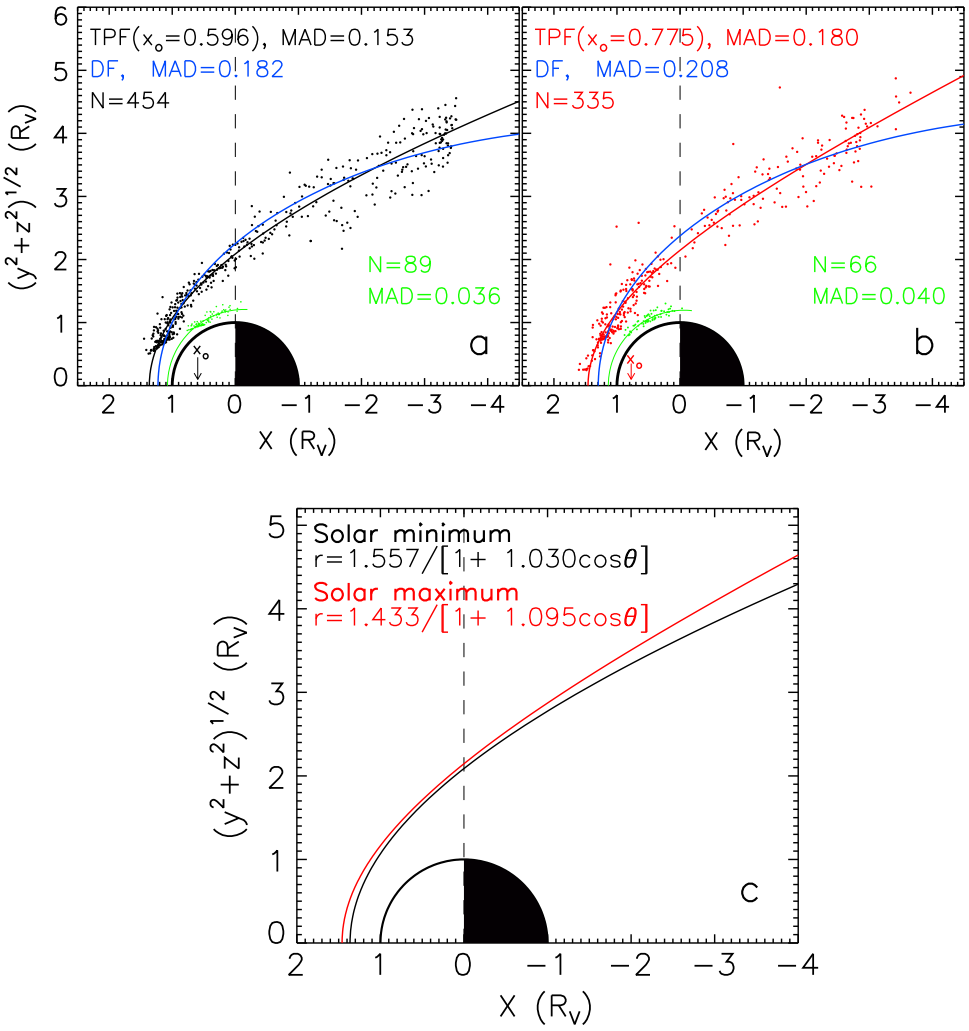

Fig. 2. Fitted curves of the Venusian bow shock and IMB location based on magnetic field measurements at solar minimum (a) and solar maximum (b) in VSO cylindrical coordinates. The MAD values are also calculated. For the bow shock, the blue curves represent the fits with DF methods, and the black and red curves are from TPF method for solar minimum and maximum, respectively. The two fitted bow shock models for solar minimum and maximum are then displayed for comparison (c). The DF fits for the IMB are also displayed in green in panels a and b. For more explanation, see text. (For interpretation of the references to color in this figure legend, the reader is referred to the web version of this article.)

Table 1
Venusian bow shock fit parameters at solar minimum and solar maximum.

	Number of crossings	$x_o(R_V)$	$L(R_V)$	ε	$R_T(R_V)$	$R_S(R_V)$	
This study	454	0.596	1.557	1.030	2.087	1.364	Solar minimum
Zhang et al. (2008)	147	0	2.14	0.621	2.14	1.32	
Martinecz et al. (2008)	248	0.788	1.303	1.056	1.984	1.422	
Russell et al. (1988)	166	0	2.14	0.609	2.14	1.33	
Slavin et al. (1984)	~66	0.45	1.68	1.03	2.10	1.28	
This study	335	0.775	1.433	1.095	2.146	1.459	Solar maximum
Zhang et al. (1990)	135	0	2.394	0.66	2.394	1.440	

accurately with plasma wave, magnetic field and electron data (Trotignon et al., 1996; Vignes et al., 2000; Bertucci et al., 2003a, 2003b). Two criteria are used for identifying the IMB only with magnetic field data: the end of fluctuations in the magnetosheath, the amplitude increase if on the dayside and rotation of magnetic field. It should be noted that VEX cannot cover the SZA range from about less than 40° at the IMB because of the orbital limitations. We have identified 89 clear crossings at solar minimum and 66 clear crossings at solar maximum. We used only partial fits of the IMB for SZA $<90°$, since the present study is focused on the bow shock location. On the dayside, as was found from previous studies at Mars (Trotignon et al., 1996; Vignes et al., 2000), the DF method provided more reliable results for IMB location than the TPF method. We won't discuss the difference between solar minimum and maximum for IMB due to the limited sample used here. A more complete analysis of the IMB location is left for a future study.

The details of the bow shock fitting results are listed in Table 1. Several previous models for the Venusian bow shock are also given. The eccentricities are 1.030 at solar minimum and 1.095 at

solar maximum, and the focus of the conic section curve changes from (0.596R_V, 0, 0) at solar minimum to (0.775R_V, 0, 0) at solar maximum. The stand-off distance (R_S) increases from 1.364R_V at solar minimum to 1.459R_V at solar maximum, while the terminator shock distance (R_T) changes from 2.087R_V at solar minimum to 2.146R_V at solar maximum. The shock is farther away from Venus at the solar maximum than at the solar minimum.

3. Discussion and conclusions

PVO observations have shown that solar activities can influence the shape of the Venusian bow shock, as the bow shock terminator distance was found to be larger at solar maximum than at solar minimum (Slavin et al., 1979b). However, the range of the SZA at the Venusian bow shock covered by PVO is limited from ~60° to ~110°(Slavin et al., 1979b), and the subsolar location cannot be well defined. The VEX mission covers a larger range of SZA (from ~10° to ~135°) at the Venusian bow shock, and both the stand-off and terminator distance of the Venusian bow shock can be accurately determined (Zhang et al., 2006). In this paper, with the TPF method, we revisit the influence of the solar activity on the shape of the Venusian bow shock based on VEX observations. The PVO observations, where the shock is farther away from Venus at solar maximum, are confirmed. The stand-off distance changes from 1.364 at solar minimum to 1.459R_V at solar maximum, and terminator shock distance changes from 2.087 at solar minimum to 2.146R_V at solar maximum. The focus of the conic section curve of the Venusian bow shock is found to change from (0.596R_V, 0, 0) at solar minimum to (0.775R_V, 0, 0) at solar maximum.

When EUV fluxes are very high and the solar wind dynamic pressure is on average quite low, any variation of the pressure will have an impact on shock positions in some ways (Russell et al., 1988). We could not calculate the dynamic pressure because of the usual lack of reliable plasma data. However, there is a proxy, which has been used at Mars by Crider et al. (2003). Their method assumes that in the pressure balance equation the contribution of the thermal pressure is neglected compared to the solar wind dynamic and magnetic pressures. Therefore, the solar wind pressure is

$$P_{ISWD} = \frac{B_{MB}^2}{2\mu_o k \cos^2\theta} \quad (2)$$

where P_{ISWD} is the inferred solar wind dynamic pressure, B_{MB} is the maximum value of the magnetic field in the magnetic barrier. μ_o is permeability and θ is the angle between the ram direction and the surface normal. Typical value 0.88 is used for the proportionality constant k.

Fig. 3a (solar minimum) and Fig. 3b (solar maximum) illustrate the dependence of the subsolar bow shock R_S on the inferred solar wind dynamic pressure P_{ISWD} derived from magnetic field data. The average subsolar shock distance $R_{S\ Ave.}$ varies from 1.36R_V to

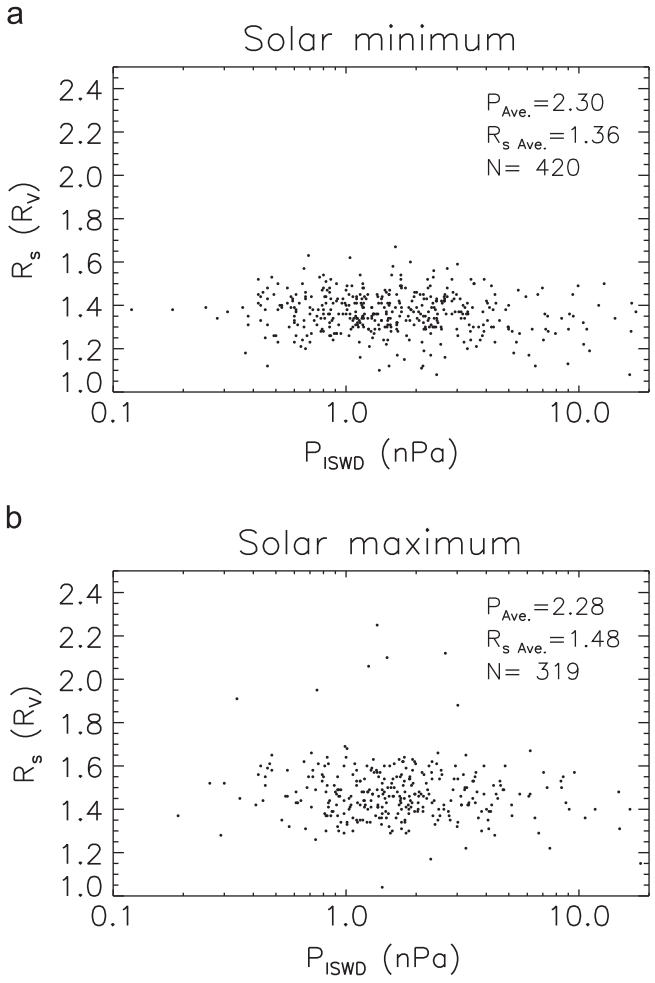

Fig. 3. The dependence of the subsolar Venusian bow shock distance on the inferred solar wind dynamic pressure at solar minimum (a) and maximum (b). $P_{Ave.}$ is the average dynamic pressure, and $R_{s\ Ave.}$ is the average of subsolar bow shock distance.

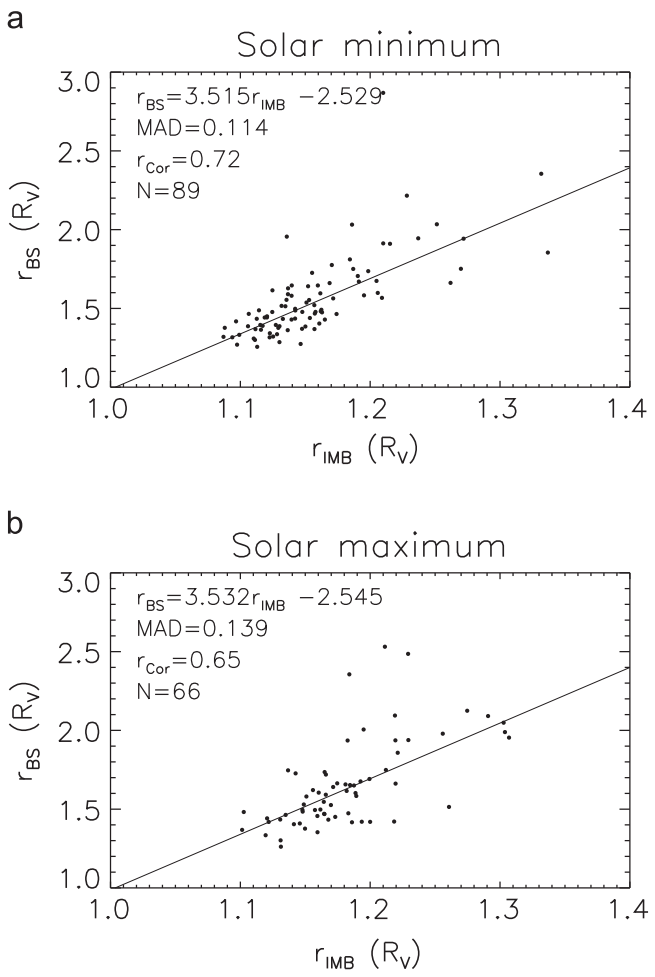

Fig. 4. The dependence of Venusian bow shock position on the induced magnetosphere boundary (IMB) location at solar minimum (a) and maximum (b). r_{BS}, r_{IMB} are bow shock and IMB distances from the center of Venus for the same orbit. r_{Cor} is the correlation coefficient of the measurements.

1.48R_V, while the average pressure $P_{Ave.}$ derived from our proxy only remains nearly constant (from 2.30 nPa to 2.28 nPa). Fig. 3a and b illustrate that despite P_{ISWD}has a large dynamic range of more than 2 orders of magnitude, there is no dependence of R_s on P_{ISWD} for both solar conditions. It should be noted that we also examined the dependence of the terminator shock distance R_T on the pressure, which provides similar results (not shown). In Fig. 3a and b, there is no evident correlation between R_S and P_{ISWD}. Therefore, our study shows that the dominating factor for the variation of the average shock position at different solar cycle phases is not the variation of solar wind dynamic pressure.

As a stretchy obstacle to the solar wind at Venus, the clear crossings of IMB on the dayside are identified. In Fig. 2, the fitted subsolar point of IMB is closer to Venus at solar minimum (1.075R_V) than that at solar maximum (1.137R_V). Fig. 4a and b illustrate clearly that, there is a positive correlation between the distances of bow shock and IMB for the same orbit. The correlation coefficients are 0.72 and 0.65, corresponding to 0.114$R_V$and 0.139$R_V$of MAD, respectively. When the solar activity is strong, solar EUV fluxes are high and more neutral particles from the Venusian ionosphere are ionized and extended into the magnetosheath due to the lack of the protection from an intrinsic magnetic field at Venus (Luhmann, 1986). As a result, the shock may move further from Venus through the mediation of the thermal pressure (Zhang et al., 1990). This is different from Mars. IMB at Mars appears as independent of solar cycle phase (Vignes et al., 2000, 2002). The distance of Mars from the Sun is over 2 times than for Venus. Compared with EUX fluxes at Venus, it is less than one in eight at Mars. So the influence of solar cycle on bow shock and IMB could be neglected at Mars contrary to Venus. Additionally, considering the size of these nonmagnetic planets, Venus is much larger than Mars. The Venusian bow shock and its induced magnetic barrier are also at larger distances than at Mars. The location of Martian bow shock perhaps has a so lower variation during different solar phases that it is difficult to identify it from observations.

In this paper, more attention are focused to the difference of shock positions at different solar phases. It is clear that the ensemble average location of the shock at solar maximum is farther away from Venus than at solar minimum. However, we can also find the small difference of the average shock locations between the VEX and PVO observations during solar maximum and minimum (Alexander and Russell, 1985; Russell et al., 1988). The average sunspot number and 10.7 cm solar radio flux (from the website: http://lasp.colorado.edu/lisird/tss/noaa_radio_flux.html) at the solar maximum and solar minimum in our study are different from those in the PVO observations, which are shown in Fig. 5. For example, the average sunspot number and 10.7 cm solar radio flux at the solar maximum during the VEX observations are 60 and 119, while at the solar maximum during the PVO observations they are about 155 and 199. At the same time, the average interplanetary conditions, which include the interplanetary magnetic field, solar wind speed, and plasma density etc., during the VEX observations have significant differences from those during the PVO observations solar cycle (Smith and Balogh, 2008; McComas et al., 2008; Luhmann et al., 2011). These effects combined with the solar activity may be the reason that leads to the difference of the average shock position between the VEX and PVO observations at solar maximum and minimum.

Acknowledgements

This research was supported by the National Science Foundation of China, Grant nos. 41174124, 41331067, 41274144, 41121003, the 973 Program (2012CB825602, 2013CBA01503), CAS Key Research Program KZZD-EW-01, and Ministry of Education (Grant no. IRT1190).

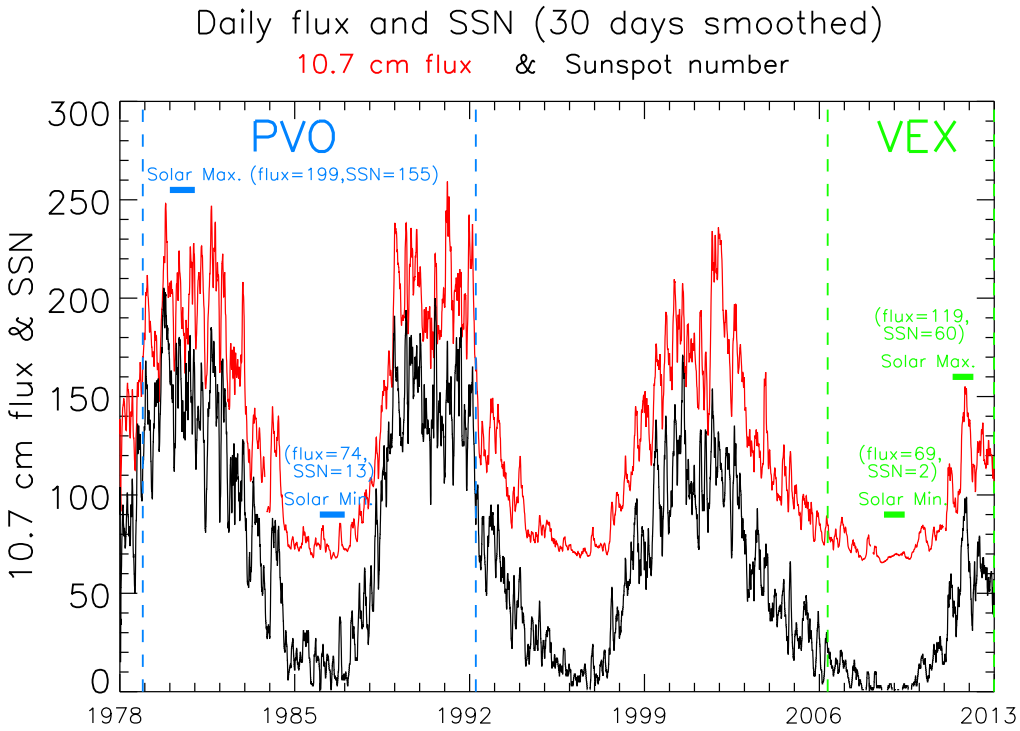

Fig. 5. The daily 10.7 cm solar radio flux (red) and sunspot number (black) during different solar cycles. The blue and green dashed lines marked the durations for PVO and VEX, respectively. Average values of the flux and sunspot number (SSN) are calculated for different solar maximum and minimum, respectively. (For interpretation of the references to color in this figure legend, the reader is referred to the web version of this article.)

References

Alexander, C.J., Russell, C.T., 1985. Solar cycle dependence of the location of the Venus bow shock. Geophys. Res. Lett. 12, 369–371.

Bertucci, C., et al., 2003a. Magnetic field draping enhancement at the Martian magnetic pileup boundary from Mars global surveyor observations. Geophys. Res. Lett. 30 (2), 1099.

Bertucci, C., Mazelle, C., Slavin, J.A., Russell, C.T., Acuña, M.H., 2003b. Magnetic field draping enhancement at Venus: evidence for a magnetic pileup boundary. Geophys. Res. Lett. 30 (17), 1876.

Bridge, H.S., Lazarus, A.J., Snyder, C.W., Smith, E.J., Davis, L., Coleman, P.J., Jones, D.E., 1967. Mariner V: plasma and magnetic fields observed near Venus. Science 158, 1669–1673.

Crider, D.H., Vignes, D., Krymskii, A.M., Breus, T.K., Ness, N.F., Mitchell, D.L., Slavin, J.A., Acuña, M.H., 2003. A proxy for determining solar wind dynamic pressure at Mars using Mars Global Surveyor data. J. Geophys. Res. 108 (A12), 1461.

Dolginov, Sh.Sh., Yeroshenko, E.G., Zhuzgov, L.M., 1968. Magnetic field investigations with spacecraft Venera 4. Kosm. Issled. 6, 562–567.

Gröller, H., Shematovich, V.I., Lichtenegger, H.I.M., Lammer, H., Pfleger, M., Kulikov, Y.N., Macher, W., Amerstorfer, U.V., Biernat, H.K., 2010. Venus' atomic hot oxygen environment. J. Geophys. Res. 115, E12017.

Lu, Q.M., Shan, L.C., Zhang, T.L., Zank, G.P., Yang, Z.W., Wu, M.Y., Du, A.M., Wang, S., 2013. The role of pickup ions on the structure of the Venusian bow shock and its implications for the termination shock. Astrophys. J. Lett. 773 (L24).

Luhmann, J.G., 1986. The solar wind interaction with Venus. Space Sci. Rev. 44, 241–306.

Luhmann J.G., Lee, C.O., Riley, P., Jian, L.K., Russell, C.T., Petrie, G., 2011. Interplanetary condition: lessons from this minimum. In: Mandrini, C.H., Webb, D.F. (Eds.), Comparative magnetic minima: Characterizing Quiet Times in the Sun and Stars, Proceeding IAU Symposium, No. 286.

Mazelle, C., 2004. Bow shock and upstream phenomena at Mars. Space Sci. Rev. 111, 115–181.

Martinecz, C., et al., 2008. Location of the bow shock and ion composition boundaries at Venus—initial determinations from Venus Express ASPERA-4. Planet. Space Sci. 56, 780–784.

McComas, D.J., Ebert, R.W., Elliott, H.A., Goldstein, B.E., Gosling, J.T., Schwadron, N.A., Skoug, R.M., 2008. Weaker solar wind from the polar coronal holes and the whole Sun. Geophys. Res. Lett. 35, L18103.

Russell, C.T., 1977. The Venus bow shock: detached or attached? J. Geophys. Res. 82 (4), 625–631.

Russell, C.T., Elphic, R.C., Slavin, J.A., 1979. Pioneer magnetometer observations of the Venus bow shock. Nature 282 (5741), 815–816.

Russell, C.T., Chou, E., Luhmann, J.G., Gazis, P., Brace, L.H., Hoegy, W.R., 1988. Solar and interplanetary control of the location of the Venus bow shock. J. Geophys. Res. 93 (A6), 5461–5469.

Shan, L.C., Lu, Q.M., Zhang, T.L., Gao, X.L., Huang, C., Su, Y.Q., Wang, S., 2013. Comparison between magnetic coplanarity and MVA methods in determining the normal of Venusian bow shock. Chin. Sci. Bull. 58, 2469–2472.

Slavin, J.A., Elphic, R.C., Russell, C.T., 1979a. A comparison of Pioneer Venus and Venera bow shock observations: evidence for a solar cycle variation. Geophys. Res. Lett. 6 (11), 905–908.

Slavin, J.A., Elphic, R.C., Russell, C.T., Wolfe, J.H., Intriligator, D.S., 1979b. Position and shape of the Venus bow shock: Pioneer Venus Orbiter observations. Geophys. Res. Lett. 6 (11), 901–904.

Slavin, J.A., Elphic, R.C., Russell, C.T., Scarf, F.L., Wolfe, J.H., Mihalov, J.D., Intriligator, D.S., Brace, L.H., Taylor Jr., H.A., Daniell Jr., R.E., 1980. The solar wind interaction with Venus: Pioneer Venus observations of bow shock location and structure. J. Geophys. Res. 85 (A13), 7625–7641.

Slavin, J.A., Holzer, R.E., 1981. Solar wind flow about the terrestrial planets 1. Modeling bow shock position and shape. J. Geophys. Res. 86 (A13), 11401–11418.

Slavin, J.A., Holzer, R.E., Spreiter, J.R., Stahara, S.S., 1984. Planetary mach cones: theory and observation. J. Geophys. Res. 89, 2708–2714.

Smith, E.J., Balogh, A., 2008. Decrease in heliospheric magnetic flux in this solar minimum: recent Ulysses magnetic field observations. Geophys. Res. Lett. 35, L22103.

Sonnerup, B.U.Ö., Scherble, M., 1998. Minimum and maximum variance analysis. In: Paschmann, G., Daly, P.W. (Eds.), In: Analysis Methods for Multi-Spacecraft Data, ISSI Scientific Reports. ESA Publications Division, Noordwijk, The Netherlands, pp. 185–220.

Spreiter, J.R., Summers, A.L., Rizzi, A.W., 1970. Solar wind flow past nonmagnetic planets—Venus and Mars. Planet. Space Sci. 18, 1281–1299.

Trotignon, J.G., Dubinin, E., Grard, R., Barabash, S., Lundin, R., 1996. Martian planetopause as seen by the plasma wave system onboard Phobos 2. J. Geophys. Res. 101 (A11), 24965–24977.

Verigin, M.I., Gringauz, K.I., Gombosi, T., Breus, T.K., Bezrukikh, V.V., Remizov, A.P., Volkov, G.I., 1978. Plama near Venus from the Venera 9 and 10 wide-angle analyzer data. J. Geophys. Res. 83, 3721–3728.

Vignes, D., Mazelle, C., Rme, H., Acuña, M.H., Connerney, J.E.P., Lin, R.P., Mitchell, D.L., Cloutier, P., Crider, D.H., Ness, N.F., 2000. The solar wind interaction with Mars: locations and shapes of the bow shock and the magnetic pile-up boundary from the observations of the MAG/ER experiment onboard Mars Global Surveyor. Geophys. Res. Lett. 27 (1), 49–52.

Vignes, D., Acuña, M.H., Connerney, J.E.P., Crider, D.H., Rème, H., Mazelle, C., 2002. Factors controlling the location of the bow shock at Mars. Geophys. Res. Lett. 29 (9), 1328.

Whittaker, I., et al., 2010. Venusian bow shock as seen by the ASPERA-4 ion instrument on Venus Express. J. Geophys. Res. 115, A09224.

Zhang, T.L., Luhmann, J.G., Russell, C.T., 1990. The solar cycle dependence of the location and shape of the Venus bow shock. J. Geophys. Res. 95 (A9), 14961–14967.

Zhang, T.L., et al., 2006. Magnetic field investigation of the Venus plasma environment: expected new results. Planet. Space Sci. 54, 1336–1343.

Zhang, T.L., 2008. Initial Venus Express magnetic field observations of the Venus bow shock location at solar minimum. Planet. Space Sci. 56, 785–789.